Title
PRISMATIC LOOPS AND CLIMB KINETIC IN QUENCHED Al-1% Ms ALLOY

Author
Kannan, V.C.

Publication Date
1965-05-01

UCRL-16090

University of California

Ernest O. Lawrence Radiation Laboratory

PRISMATIC LOOPS AND CLIMB KINETICS IN QUENCHED Al-1% Mg ALLOY

Berkeley, California

UCRL-16090

UNIVERSITY OF CALIFORNIA

Lawrence Radiation Laboratory
Berkeley, California

Contract No. W-7405-eng-48

PRISMATIC LOOPS AND CLIMB KINETICS IN QUENCHED Al-1% Mg ALLOY

V. C. Kannan

May 1965

DISCLAIMER

Contents

PRISMATIC LOOPS AND CLIMB KINETICS IN QUENCHED Al-1% Mg ALLOY

V. C. Kannan

Department of Mineral Technology, College of Engineering
University of California, Berkeley, California

May 1965

ABSTRACT

Annealing of loops in quenched Al-1% Mg alloy has been studied by hot-stage electron microscopy. The activation energy for loop climb has been estimated to be 1.2 - 1.28 e.V., which is in the same range as that found for pure aluminum. The absence of heterogeneous precipitation of vacancies, and the bulk annealing results showed that the binding energy between magnesium atoms and vacancies, in the present alloy, is very small. It is concluded that $\frac{\%\ \text{supersaturated solute atoms}}{\%\ \text{vacancy}}$ ratio primarily determines whether positive or negative climb can take place in a given alloy. The stacking fault energy was estimated by comparison of the shrinkage rates of perfect and imperfect loops as ~190 ergs/cm^2 at 207°C.

I. INTRODUCTION

The concentration of vacancies C_v in thermal equilibrium in a metal varies with temperature T as:

$$C_v = C_o e^{-E_f/kT} \qquad (1)$$

where E_f is the energy of formation of a vacancy and k the Boltzman constant. For aluminum, E_f is known to be 0.76 e.V.[1] and taking $C_o \sim 1$, the vacancy concentration is 10^{-4} at the melting point (923°K) and 10^{-13} at room temperature. By rapidly quenching from near the melting point, it is possible to retain most of the vacancies ($\sim 10^{-4}$) in supersaturation.

The subsequent annealing of quenched-in vacancies in FCC metals and alloys has received much attention during the past few years.[2,3,4] Many physical and mechanical properties such as electrical resistivity, internal friction, yield stress, etc., are much influenced by the annealing of vacancies. Transmission electron microscopy has been used to study mechanisms of vacancy elimination by several workers (for a review see ref. 5). All the experiments done so far confirm in a general way the earlier postulation of Kuhlman-Wilsdorf[6] that vacancies should attract to form clusters and subsequently collapse to form loops of dislocations on {111}. There is a large driving force (the chemical force due to supersaturation in the case of Al is ~300 kgm/mm^2) by which the supersaturation is eliminated by the migration of vacancies to sinks such as surfaces, grain boundaries and dislocations as well as by the formation of dislocation loops.

The type of loop that is formed depends upon the stacking fault

energy. However, this can assume secondary importance because of all the complications that can arise which affect the nucleation and growth of loops, such as plastic deformation, quenching stresses, impurities, etc.[5-10] Thus, in pure aluminum, if quenching is performed without deforming the specimen, very large Frank loops (i.e. $\vec{b} = \frac{1}{3}\langle 111\rangle$) well in excess of that expected from stacking fault energy considerations are observed.[11] If, on the other hand, deformation is purposely allowed to take place during quenching, loops are usually of the perfect type[12] (i.e. $\vec{b} = \frac{1}{2}\langle 110\rangle$). As will be shown in this thesis, the same is true for Al-1% Mg alloy; hence, impurities alone cannot account for the existence or non-existence of Frank loops as has been suggested by Cotterill and Segall.[8]

Many experimental results suggest that the conversion of a Frank loop to a perfect loop by nucleation of a Shockley partial:

$$\frac{1}{3}[111] + \frac{1}{6}[11\bar{2}] = \frac{1}{2}[110]$$

is stress-aided. Since the energy of a dislocation line is ~5 e.V. per atom, it would be extremely difficult to nucleate a Shockley partial spontaneously and this explains why very large Frank loops are observed in Al and Al-Mg alloys after careful quenching; since, if the activation energy for nucleation of a Shockley partial is neglected and taking $\gamma_{SF} = 300$ ergs/cm^2 for aluminum, no Frank loop > 200Å should be observed. Actually, loops > 1000Å are often seen in aluminum and its alloys if careful quenching procedures are adopted (see Figs. 4c,d).

The perfect loop on a (111) is not a stable equilibrium configuration. Both theory[13] and experiments[12,14] show that during growth, a loop can rotate on its glide cylinder while climbing, leading to the

formation of diamond loops of nearly edge character with probable habit plane near {110} depending on its size. In aluminum and its alloys, these diamond shaped loops can be observed in as-quenched specimens, thereby suggesting that loop growth can occur during or immediately after quenching. The size and the type of loops are also influenced by aging time and treatment. Many of these and other points pertinent to quenching experiments have been reviewed recently by Thomas and Washburn.[5]

Besides providing information on the nature and geometry of dislocation loops, the electron microscope can be used to determine the kinetics of climb processes by annealing the thin foils in situ (i.e. by hot stage electron microscopy). In the case of pure aluminum, loops are always observed to shrink during heating above 150°C because the nearby free surface provides an infinite-vacancy-sink, i.e. no supersaturation is possible.[4] The rate of shrinkage at various temperatures enables an estimate to be made of the activation energy of loop climb. In the case of aluminum alloys, provided both solute atoms and vacancies are in supersaturation, it has been observed that loops can grow during annealing of thin foils indicating that a large vacancy supersaturation can remain after quench-aging.

The kinetics are then different from aluminum, since the solute-vacancy binding energy perturbs both the energy of formation of vacancy E_f and its migration energy E_m.[14] In Al-5% Mg alloy, the activation energy for loop growth was determined to be 0.95 e.V. as compared to 1.2-1.3 e.V. for that of pure aluminum.[4] Eikum and Thomas found E_b to be about 0.2 e.V. in Al-5% Mg alloys,[17] a result confirmed by other workers.[15,16]

From the foregoing paragraphs, it can be seen that it is necessary to examine whether or not supersaturation of solute atoms, i.e. the ratio of $\frac{\%\ \text{solute}}{\%\ \text{vacancies}}$ is important in controlling the climb processes. As can be seen from Fig. 1, for Al-Mg alloys, this requires an alloy of aluminum with < 2% of Mg. For the present work, Al-1% Mg was prepared. Other factors investigated were (1) the conditions under which principally perfect or imperfect loops are formed, (2) estimation of stacking fault energy.

II. EXPERIMENTAL PROCEDURE

A. Preparation of the Alloy

The alloy was prepared from 99.999% pure aluminum and 99.995% Mg supplied by United Mineral and Chemical Corporation. A casting mold made of reactor grade graphite was used to cast the alloy ingots of $11" \times \frac{3}{4}" \times \frac{3}{8}"$. The use of a high frequency induction furnace allows one to reach any temperature at a relatively high rate. Since both aluminum and magnesium have little difference in atomic weight and nearly the same melting points, little segregation problems are incurred though many precautions were taken to avoid such effects. The graphite mold was degassed at 1000°C at 6×10^{-6} mm of Hg for $\frac{1}{2}$ hour. The charge was melted in an atmosphere of pure helium at 5 atm pressure that had been passed through activated charcoal filters and a nitrogen trap to remove moisture. The melting was carried out for 20 min. at 670°C. Then the power was cut off and fresh cold helium was let in to hasten solidification. Trial runs were carried out to find optimum conditions.

The ingot was rolled into thin strips of 12-6 mil thick, cleaned

with acetone after each pass. This ensures a clean and smooth surface and is beneficial for subsequent specimen preparation.

B. Specimen Preparation

Specimens of 6" x 1" x 12-6 mil were all held at 650°C for 12 hours at partial vacuum. Chemical analyses were subsequently carried out and the compositions are listed in Table I. This annealing treatment prior to quenching is important to reduce the dislocation density to a minimum and to provide specimens of the same initial state.

The 6" strips were cut into six one inch specimens and placed in a specimen holder designed to minimize the deformation of the foil during quenching. Specimens were held at 545°C in a furnace which has a vertical slot at the bottom of 7.5 cm x 7.5 cm x 0.32 cm. The hot zone was kept as near to the quenching bath as possible. Quenching was carried out by pulling the specimen holder into a long vertical column containing the quenching medium (oil or water) both kept right under the hot zone just prior to quenching. The specimen was held in the furnace for 1 hour to ensure uniform homogenization of temperature. This arrangement provides a satisfactory rapid quench, quick transfer of the specimen from furnace to bath, and also avoids bending of the specimen while quenching. Specimens were quenched into silicone oil bath or water at 45°C as will be described at appropriate places. Aging just after quenching at room temperature was the same for all specimens unless otherwise stated.

C. Preparation of Thin Foils

Specimens were electropolished at-25°C using a mixture of 110 cc perchloric acid (70%) and 480 cc of 200 proof ethyl alcohol. A stainless

steel beaker served as a cathode. The specimen (anode) was suspended from a clamp into the bath. The polishing was carried out at 30V and 0.12 amps.

A modified window technique was employed to produce thin foils. Specimens were polished and turned upside down soon after holes were first formed at the top of the window. Three or four such repetitions gave uniformly thin specimens. During final polishing, as soon as holes were observed to form, the current was switched off and on, during which thin foils are ejected out of the specimen. The foils were removed from the beaker, washed in absolute alcohol and mounted for observation in the electron microscope.

D. Bulk Annealing

Specimens after quenching from various temperatures were bulk annealed before polishing to compare with the results for concentrated aluminum-magnesium alloys obtained in our laboratory previously.[17] Factors such as pre-aging time, quenching and polishing conditions were kept the same for all the specimens. A constant temperature glycerine bath was used for bulk annealing. Thin foils were obtained by electro-polishing as described earlier.

E. Hot-State and Ciné Photography

Thin foil annealing experiments were carried out using a Siemens heating stage in the Siemens Elmiskop Ib. A 12 volt storage battery or a constant voltage power supply served as a power source. Current to the platinum furnace was regulated through a variable resistance and the temperature was read from the calibration curve shown in Fig. 2. Details of the calibration procedures are described in the appendix.

The climb of loops was recorded using a Paillard-Bolex H1b movie camera driven at 12 frames/sec. A Bell and Howell f 0.95 lens, fully open, was used. Tri X movie films were found to give the best results. During heating, the beam current was kept at 10μ amp just at the time of exposure. This gives a maximum possible accurate temperature reading, since the beam itself does not cause much heating if the normal precautions are observed.[18]

Selected area diffraction patterns were taken initially and at the end of the experiment so that any changes in orientation could be followed during heating. All the climb experiments recorded were done in bright field.

Actually, it is better to do annealing experiments in dark field (two beam case, $s = 0$), by tilting the gun so that the desired diffraction spot can be brought to coincide with the optical axis. This minimizes the aberration errors and gives sharp contrast. The advantage of the above method over the bright field is that there is an increase in contrast due to removal of much of the inelastically scattered electrons (at higher angles, inelastic scattering is less).

By tilting the gun the same diffraction condition can be maintained, i.e. $s = 0$, while heating the foil (bright or dark field) since the Siemens specimen stage is non-tiltable. This eliminates any change in size of the loop due to variation in diffraction condition. Loop size depends upon the diffraction condition, as the image of a dislocation line falls to one side or the other of the true position, depending upon whether $(\bar{g}.\bar{b})s$ is positive or negative. A discussion of these and other factors related to high temperature work is given in ref. 18. However,

from a practical point of view, at least two persons are required to carry out such experiments, and in this work bright-field imaging was adopted taking precautions to maintain constant diffraction conditions.

III. EXPERIMENTAL RESULTS AND INTERPRETATION

A. Non-supersaturation of Vacancies

Bulk annealing of specimens of ~8 mil thick was carried out at room temperature for 24 hours and at 45°C, 175°C and 200°C for 5 minutes each. All specimens were quenched into silicone oil at 20°C from 545°C and pre-aged at 20°C for 10 minutes before bulk annealing. Specimens were prepared from bulk annealed samples by electropolishing as described earlier. Typical micrographs are shown in Fig. 3.

It can be seen that loops are formed at random showing no evidence for heterogeneous precipitation, i.e. no helices or climb sources are observed. The vacancy concentration C_v' can be calculated from these micrographs as follows: If N is the number of loops per cm^3 and r the radius, then

$$C_v' = \pi r^2 b N \qquad (2)$$

where $\bar{b}$ = Burger's vector = $\frac{a}{2}\langle 110\rangle$ for a perfect loop and $\frac{a}{3}\langle 111\rangle$ for a Frank loop.

In using this formula, the thickness of the specimen was assumed to be 3000Å in all cases, based on the determinations from slip traces, in some foils, after prolonged observation. According to the $\bar{g}.\bar{b}$ criterion, loops will be either visible or invisible according to whether the above mentioned scalar product is zero or non-zero. All the micrographs in Fig. 3 are in [001] orientation. For a particular

operating reflection $\bar{g}_2$, the various $\bar{g}.\bar{b}$ values for both Frank and perfect loops can be tabulated as shown in Table II. Assuming equal probability of formation of all possible loops of $\frac{1}{2}$ <110> (or $\frac{1}{3}$ <111> in case of Frank loops), those not visible due to contrast effects can be accounted for.

The vacancy concentrations C_v' are calculated using Eq. 2, and the values are tabulated in Table III. These values include corrections for those loops which are invisible.

Using Eq. 1 for Al-1% Mg alloy and taking E_f as 0.76 as in the case of pure aluminum, we get $C_v' \sim 0.2 \times 10^{-4}$. This value is in the same range as those listed in Table III. This clearly indicates the absence of too much influence of soluble Mg atoms on the energy of formation of a vacancy.

The results of Table III also indicate the absence of supersaturation of vacancies in this particular alloy. Comparison of the above results with those obtained for Al-5% Mg alloy by Eikum and Thomas[17] shows clearly the following. In Al-5% Mg alloy, C_v' increased from 10^{-5} to 10^{-3} by bulk annealing a quenched specimen at 180°C for 5 minutes. In the present case no such increase is seen. Thus, $\frac{\%\text{ supersaturated solute atoms}}{\%\text{ vacancy}}$ ratio determines whether or not vacancy supersaturation can exist in a specimen.

Lomer[19] has derived an equation for C_v' in the case of a two component system as:

$$C_v' = Ae^{-E_f/kT}\,(1 - 12C + 12C\,E_b/kT) \qquad (3)$$

where E_b is the binding energy between a solute atom and a vacancy; C the atomic fraction of solute atoms and all other symbols are defined

in the text earlier. But, in the case of Al-1% Mg alloy, the vacancy concentration is nearly equal to that of pure aluminum. Thus, the Lomer's equation can be modified as follows:

$$C_v' = Ae^{-E_f/kT}\{1 - 12C' + 12C' e^{E_b/kT}\} \qquad (4)$$

where the new symbol C' denotes the concentration of supersaturated solute atoms, i.e. $C' = C - C_o$ where C is the actual atomic fraction of solute atoms and C_o, the velue of maximum solubility of solute atoms at room temperature. In the case of Al-Mg alloys, C_o is ~2% [see Fig. 1]. Thus, for non-saturated alloys Eq. 4 reduces to Eq. 1 assuming no entropy change.

B. Effect of Quenching Conditions on Loops

By varying the quenching rates (e.g. by quenching in different media or changing specimen thickness) it was found that for minimum plastic deformation during quenching, the predominant defects were Frank loops. This is illustrated in Fig. 4. It can be seen that the Frank loops are much more predominant in oil quenching than in water-quenching. Since water-quench introduces much more quenching-stresses into the specimen than that of oil-quench, we see that Frank loops are retained if quenching-stresses are kept at a minimum.

The results confirm the previous work on pure aluminum[12] and shows that it is the quenching conditions and not the solute atoms which primarily determine the type of loop that forms on quenching. Thus, the conversion of a Frank to a perfect loop by the nucleation of a Shockley partial is stress-aided, i.e. Frank to perfect loop conversion occurs heterogeneously. This conclusion can also be inferred from Fig. 4. For fast quenches (into water) the loop nucleation rate is

higher than for slow quenches (compare b with c and d) and so after water-quenching the stress fields from close neighboring loops may also assist in the Frank → perfect loop transformation. This effect is not so significant when the nucleation rate is much less.

Cotterill and Segall[8] have reported that in the case of 99.98% pure aluminum, Frank loops were seen only after repeated quenchings. In the case of high purity aluminum, very large Frank loops were commonly seen after a single quench. In the case of the present alloy, Frank loops were seen after a single quench even though 1% of Mg atoms are present. A possible explanation for this behavior can be given as follows. In the case of impure aluminum used by Cotterill and Segall, the impurities may have been insoluble and hence could act as sites for heterogeneous nucleation of vacancy clusters. However, in the case of the alloy investigated here, magnesium dissolves completely forming a single phase solid solution and does not provide any sites for heterogeneous precipitation of vacancies. It also follows from the present results that magnesium cannot lower the stacking fault of aluminum sufficiently to allow easy conversion of a Frank to a perfect loop. Thus, the behavior of Al-1% Mg alloy and pure aluminum is similar.

C. Dynamic Observations of Climb

Without exception, all the loops were seen to shrink on annealing in situ. The loop climb was recorded by taking motion pictures at various temperatures. Figure 5 shows a sequence of shrinking loops at ~190°C, and Fig. 6 shows negative climb of Frank loops at ~170°C. It can be seen that some Frank loops shrink without unfaulting in this micrograph. However, it is also observed that Frank loops unfault

before disappearing (e.g. at B, Fig. 6). This can be understood if it is assumed that in the latter case localized stresses cause nucleation of a Shockley partial leading to unfaulting. When the foil is heated to high temperature in between two grids, the thermal expansion of the specimen may induce mechanical stresses in the foil.

Again, in cases where Frank loops are unfaulted before completely disappearing while heating, it is also seen that loops appear to become larger under the same diffracting conditions when unfaulting took place (Fig. 7). Although a loop can rotate after unfaulting to change its habit plane and thus its projected area on the micrograph may be affected, this alone cannot explain such a large change in diameter in this case, particularly as the foil has not tilted during the sequence. On the other hand, this may be due to release of stacking fault energy, which is similar to surface tension. The shape and size of the loop is determined by the equilibrium between stacking fault energy, elastic interaction energy of opposite sides of a loop, elastic field energy and any other internal stress-fields. Since stacking fault energy acts in such a way so that the loop assumes a smaller diameter, its release may tend to make the loop to acquire large diameter; but, in actual cases, expansion of the loop could be due to the cumulative effects of unfaulting and loop rotation.

D. Activation Energy for Loop Climb

Without exception, all loops were observed to shrink on annealing thin foils at temperatures higher than 180°C. Silcox and Whelan[4] were the first to study annealing of loops in pure aluminum. They showed that loops, shrink by emitting vacancies which migrate to nearby sinks, e.g. free surfaces and grain boundaries.

The loop climb was interpreted in terms of Friedel's theory[20] of movement of jogs. The velocity of a jog along a dislocation is given by

$$V_c = \frac{Z \nu_a b}{\sin \varphi} \exp\left(-\frac{E_f + E_m}{kT}\right)\left[\exp \frac{F_c b^2}{kT} - \exp \frac{F_s b^2}{kT}\right] \qquad (5)$$

where $Z \sim 11$, the atomic coordination number ν_a the atomic frequency ($\sim 10^{13}$), b the Burger's vector (2.86Å for a perfect loop in Al). E_f and E_m are the energies of formation and migration of the vacancy, respectively. This expression neglects the entropy term. F_s is the chemical force due to supersaturation of vacancies and is equal to $\frac{kT}{b^2} \log \frac{c}{c_o}$. As all the loops were observed to shrink, the supersaturation of vacancies is zero. An approximate expression for F_c is taken as

$$F_c = \frac{G b}{4 \pi (1-\sigma)} \frac{\log(r/b)}{r/b} \qquad (6)$$

where G is the bulk modulus (2.53×10^{11} cynes/cm^2), σ is Poisson's ratio and r the radius of the loop. For a circular loop lying on a (111) plane, Silcox and Whelan simplified the above equations and obtained

$$\frac{dr}{dt} = -\frac{1}{2} Z \nu_a b \exp\left(\frac{-E}{kT}\right)\left[\exp \frac{F_c b^2}{kT} - 1\right] \qquad (7)$$

On approximating $\exp \frac{F_c b^2}{kT} - 1$ as $\frac{\alpha b}{r}$ where α is a variable parameter, by substitution and then integration

$$r = r_o \left(1 - \frac{t}{\tau}\right)^{\frac{1}{2}} \qquad (8)$$

where

$$\tau = \tau_o \exp\left(\frac{E}{kT}\right)$$

and

$$\tau_o = \frac{r_o^2}{Z \nu_a b^2 \alpha}$$

Thus, a plot of radius versus time will be parabolic. The approximate values of the parameter α at various temperatures can be estimated since $\alpha \sim \frac{F_c b^2}{kT} \frac{r}{b}$ and are listed in Table IV.

From the above formula, the value of the activation energy E can be obtained by plotting r versus time as shown in Figs. 10a,b,c. The values obtained for E are given in Table IV.

The possible sources of error in this experiment are (1) uncertainty in temperature, and (2) the effect of magnesium atoms on the jog energy of the dislocation is neglected.

The first of the objections can be ignored inasmuch as the effect of temperature in estimating climb energy is very small, e.g. a variation of 10°C in temperature affects E by only 2%. The assumption that magnesium atoms do not affect the jog energy need not be correct since Suzuki locking is possible. However, the main effect may be only to perturb E_m and E_f and hence the value that is estimated is the perturbed value. The results show that the perturbation is small as E was found to be in the range of 1.2 - 1.28 e.v. (as was the case for pure aluminum[4]). Unless the diffraction conditions are kept constant the apparent loop size may change.[18] This can be avoided by suitable gun tilting where necessary.

The values of E calculated at various temperatures leave little doubt that the annealing of loops in Al-1% Mg alloys follows similar kinetics to that of pure aluminum. Further, there was no evidence for heterogeneous precipitation of vacancies such as helices, climb sources, rows of loops, etc. From this, one can conclude that binding energy between magnesium atom and vacancy is neglibibly small and only

$\frac{\%\ \text{supersaturated solute}}{\%\ \text{vacancy}}$ ratio is important in deciding whether positive or negative climb will occur on annealing thin foils. This conclusion is in excellent agreement with Beaman and Balluffi,[21] who measured the binding energy as ≤ 0.01 e.V. in Al-0.56% Mg and Al-1.11% Mg alloys.

From the foregoing paragraphs and the conclusions drawn therefrom, it is interesting that a possible variation of activation energy for loop climb with magnesium concentration can be predicted. Since the room temperature saturation is ~2 atomic % magnesium, one might observe a sudden drop in activation energy at this concentration.[18] This is illustrated in Fig. 11.[18] The experimental points do not disagree with this possibility.

E. Stacking Fault Energy

Figures 8 and 9 show sequences of shrinkage of both perfect and imperfect loops in the same area. It is seen that Frank loops shrink at a faster rate than the perfect loop. An estimation of stacking fault energy can be made by determining the ratio of the rates of shrinkage of perfect loops and imperfect loops at the same temperature.

For a circular loop enclosing the stacking fault, the energy E is given by

$$E = \frac{G\,b^2}{4\pi(1-\nu)}\,\ell n\left(\frac{r_o}{b}\right).\,2\pi r + \pi r^2\,\gamma \qquad (9)$$

where r is the loop radius, γ the stacking fault energy and all other symbols have been defined earlier, $|\bar{b}|$ is 2.36Å for an imperfect loop. r_o is taken to be equal to $|\bar{b}|$ and core energy has been neglected.

From this we see that Eq. 3 can be modified for the shrinkage of an imperfect loop as follows. The stacking fault energy γ will assist

the climb in addition to the climb force F_c due to line tension. Then we can write Eq. 5 as

$$\left(\frac{dr}{dt}\right)_{\text{Imperfect}} = \frac{1}{2} Z \nu_a b \exp\left(\frac{-E}{kT}\right) \left[\exp\frac{(F_c + \gamma)b^2}{kT} - 1\right] \qquad (10)$$

For loops of the sizes observed in this work, the energy due to the fault far exceeds that due to dislocation line tension and hence we can take F_c as zero in comparison to γ in the Eq. 10. This is valid until the loop diameter becomes small, i.e. for the initial stages of shrinkage. With this approximation, then from Eqs. 5 and 10 we get

$$\frac{(dr/dt)_{\text{imperfect}}}{(dr/dt)_{\text{perfect}}} = \frac{\exp\left\{\frac{\gamma b_i^2}{kT}\right\} - 1}{\exp\left\{\frac{F_c b_u^2}{kT}\right\} - 1}$$

Thus, we see that this method does not require a knowledge of the self-diffusion energy, nor of the entropy factor. Calculation at 207°C and 220°C shows a value of ~190 - 195 ergs/cm^2 in the present alloy.

Edington and Smallman[22] investigated the annealing behavior of faulted loops in pure aluminum. The annealing experiments were conducted in the electron microscope. From shrinking sequences of only faulted loops at one temperature, they measured the stacking fault energy for an intrinsic fault at 165°C as 280 ± 50 ergs/cm^2. At the same temperature, they measured the climb rate of an imperfect loop with an extrinsic fault and calculated the energy of an extrinsic stacking fault as 420 ergs/cm^2. By comparison with the present results, it is seen that magnesium in dilute Al-Mg alloys may have a small effect in lowering the stacking fault energy of pure aluminum.

IV. CONCLUSIONS

1. Annealing of loops in thin foils in situ in quenched Al-1% Mg alloy follows similar kinetics to those found previously for pure aluminum. The activation energy for loop climb in the present alloy was estimated to be 1.2 - 1.28 e.V., which is in the same range as that found for pure aluminum.[4]

2. The absence of heterogeneous precipitation of vacancies and the bulk annealing results show that the binding energy between magnesium atoms and vacancies is very small in this alloy. This is in excellent agreement with the values of Balluffi and Beaman[21] determined by equilibrium measurements.

3. A possible prediction of variation of activation energy of loop climb with magnesium is quite possible. Since $\frac{\%\ \text{supersaturated solute atoms}}{\%\ \text{vacancy}}$ ratio determines whether positive or negative climb can take place, it is concluded therefore that solute atoms in supersaturation are responsible for loop growth in concentrated Al-Mg alloys. Since the supersaturation limit of magnesium in aluminum is 2 at.% at room temperature, there should be a variation of activation energy both with solute content > 2% (as suggested in Fig. 11) and with annealing temperature below the solvus.

4. Estimation of stacking fault energy by comparison of rates of shrinkage of perfect and Frank loops gave the values ~ 190 and ~ 199 ergs/cm^2 at 207°C and 220°C, respectively.

ACKNOWLEDGMENTS

The author expresses his deep gratitude to Professor Careth Thomas for his continued interest, encouragement and patient guidance and to Professor Jack Washburn for his valuable suggestions during the initial stages of this work. This work was supported under the auspices of the U. S. Atomic Energy Commission through the Inorganic Materials Research Division of the Lawrence Radiation Laboratory, Berkeley, California.

APPENDIX

A. Calibration of Hot Stage

The hot-stage was calibrated outside the microscope for various reasons: (1) the calibration curve supplied by Siemens is only a general one and may not hold for each particular stage, (2) a steady temperature was not reached by the specimen unless at least 10 minutes elapsed after switching on, (3) the temperature attained by the specimen depends on the position of the grid, specimen, etc. For these reasons, the stage was calibrated in the following way.

The stage was mounted inside an evaporator under a vacuum of 5×10^{-6} mm of Hg. A chromel alumel thermocouple was used to measure the thermal emf across a very sensitive potentiometer bridge. The temperature was measured in the same position where the specimen is mounted during annealing experiments. Terminal drops were extremely low as confirmed by repeating checking of the resistance of the furnace (hot-stage furnace) windings at the far end of the lead wires. Repetition of the calibration 3 or 4 times confirmed the reproducibility of the results. The calibration curves are shown in Fig. 2.

Temperature versus time was recorded at various constant input of power from 0.2 to 1.0 W in 0.1 watt steps and at 1.5 W and 2.0 watts. Since the furnace resistance increases on heating, manual control of power is needed. This is important only during the first minute of heating, since, after this time the change of resistance is small and slow. The temperatures measured were accurate to 0.5°C. However, in the microscope, beam heating cannot be neglected, so that the accuracy of temperature measurement is ±10°C. Beam heating is highly minimized

at temperatures above 150°C. Further, the beam current was turned on only after the movie camera was started.

References

1. F. J. Bradshaw and S. Pearson, Phil. Mag. 2, 379, 570 (1957).

2. T. Federighi, Phil. Mag. 4, 502 (1959).

3. W. Desorbo and D. Turnbull, Acta Met. 7, 83 (1959).

4. J. Silcox and M. J. Whelan, Phil. Mag. 5, 1 (1960).

5. G. Thomas and J. Washburn, Rev. of Mod. Phys. 35, 4, 992 (1963).

6. D. Kuhlman-Wilsdorf and H. G. F. Wilsdorf, J. Appl. Phys. 31, 516 (1960).

7. R. Vandervoort and J. Washburn, Phil. Mag. 5, 24 (1960).

8. R. M. J. Cotterill and R. L. Segall, Phil. Mag. 8, 1105 (1963).

9. J. Strudel and J. Washburn, Phil. Mag. 9, 491 (1964).

10. J. Strudel, F. Vincotte and J. Washburn, J. of Appl. Phys. 3, 148 (1963).

11. S. Yoshida, M. Kiritani and Y. Shimomura, J. of Phys. Soc. Japan 18, 175 (1963).

12. G. Das, M. S. Thesis, University of California, Berkeley. UCRL-11188.

13. R. Bullough and A. J. E. Foreman, Phil. Mag. 9, 315 (1964).

14. A. Eikum and G. Thomas, J. Appl. Phys. 34, 3363 (1963).

15. J. Takamura, K. Okazaki and I. G. Greenfield, J. of Phys. Soc. Japan, 18, Suppl. III, 78 (1963).

16. J. D. Embury and R. B. Nicholson, Acta Met. 11, 347 (1963).

17. A. Eikum and G. Thomas, J. Phys. Soc. of Japan, 18, Suppl. III, 98 (1963).

18. G. Thomas, High Temperature Electron Microscopy, AIME Symposium on High Temperature Metallography, Chicago (1965), in press.

19. W. M. Lomer, Vacancies and Other Point Defects in Metals and Alloys, Inst. of Metals Monograph and Report Series, London, 79 (1958).

20. J. Friedel, Les Dislocations (Paris, Gauthiers-Villars), (1956).

21. D. R. Beaman and R. W. Balluffi, "Measurement of Equilibrium Vacancy Concentration in Dilute Aluminum Magnesium Alloys", to be published.

22. J. D. Edington and R. W. Smallman, private communication.

FIGURE CAPTIONS

Figure 1 Aluminum - Magnesium phase diagram.

Figure 2 Time-temperature calibration curve for Siemens hot-stage at various constant power in-put.

Figure 3 Typical micrographs from foils after oil quenching (20°C) from 550°C. Specimen thickness 6.5 - 7.0 mil.

a) annealed at room temperature for 10 minutes.

b) annealed at 45°C for 10 minutes.

c) annealed at 175°C for 10 minutes.

d) annealed at 200°C for 10 minutes.

Figure 4 Typical micrographs of (a) water quenched specimen aged at room temperature for 24 hours, (b) same as (a) but no aging (c) and (d) oil quenched and aged for 24 hours (specimens are ~13 mil thick).

Figure 5 A sequence of shrinking loops at ~190°C. The time (in seconds) is given for each micrograph. Two loops A and B interact while shrinking.

Figure 6 Shrinkage of Frank loops at ~170°C showing that some faulted loops (A) do not unfault while shrinking whilst others at (B) do.

Figure 7 Heating sequence showing the apparent increase in loop size (A) during unfaulting. The diffraction conditions are the same as seen from the uniform contrast in the four photographs. The time (in seconds) is given for each micrograph.

Figure 8 Shrinkage of both perfect and imperfect loops at ~207°C. The time (in seconds) is given for each micrograph.

Figure 9 Shrinkage of both perfect and imperfect loops at 220°C. The time (in seconds) is given for each micrograph.

Figure 10 (A,B,C) Time - radius plots at various temperatures as indicated in the graphs. The experimental data has been fitted to a parabola.

Figure 11 A possible variation of activation energy for loop climb in aluminum as a function of magnesium content.

TABLE I

Alloy	Mg	Cu	Mn	Fe	Si
A	1.01%	<100 ppm	<100 ppm	<200 ppm	<200 ppm
B	0.91%	"	"	"	"

TABLE II

$\vec{b}$	$\vec{g} = 200$	$\vec{g} = 220$
$\frac{1}{3}[\bar{1}11]$	-2/3	0
$\frac{1}{3}[1\bar{1}1]$	2/3	0
$\frac{1}{3}[11\bar{1}]$	2/3	4/3
$\frac{1}{3}[111]$	2/3	4/3
$\frac{1}{2}[101]$	1	1
$\frac{1}{2}[110]$	1	2
$\frac{1}{2}[011]$	0	1
$\frac{1}{2}[\bar{1}10]$	-1	0
$\frac{1}{2}[\bar{1}01]$	-1	-1
$\frac{1}{2}[1\bar{1}0]$	-1	0

TABLE III

Treatment	Loops/cm^3	Average dia. Å	C_v'
A. Quenched in oil at 20° from 550°C			
(i) as-quenched	$\sim 4 \times 10^{13}$	1000Å	0.31×10^{-4}
Bulk-annealed at			
(ii) 45°C 5 mts	2×10^{13}	1200Å	0.4×10^{-4}
(iii) 175°C 5 mts	6.32×10^{12}	1500Å	0.28×10^{-4}
(iv) 200°C 5 mts	4.34×10^{12}	1800Å	0.28×10^{-4}
B. Water quenched 550°C annealed at room temp. 24 hrs.	8.4×10^{13}	750Å	$\sim 1.8 \times 10^{-4}$

TABLE IV

Temp. °C	α	Activation Energy E e.V.	Stacking Fault Energy γ ergs/cm^2
180	64	1.21	--
207	62	1.28	~190
220	60	1.21	~195
256	55	1.20	--

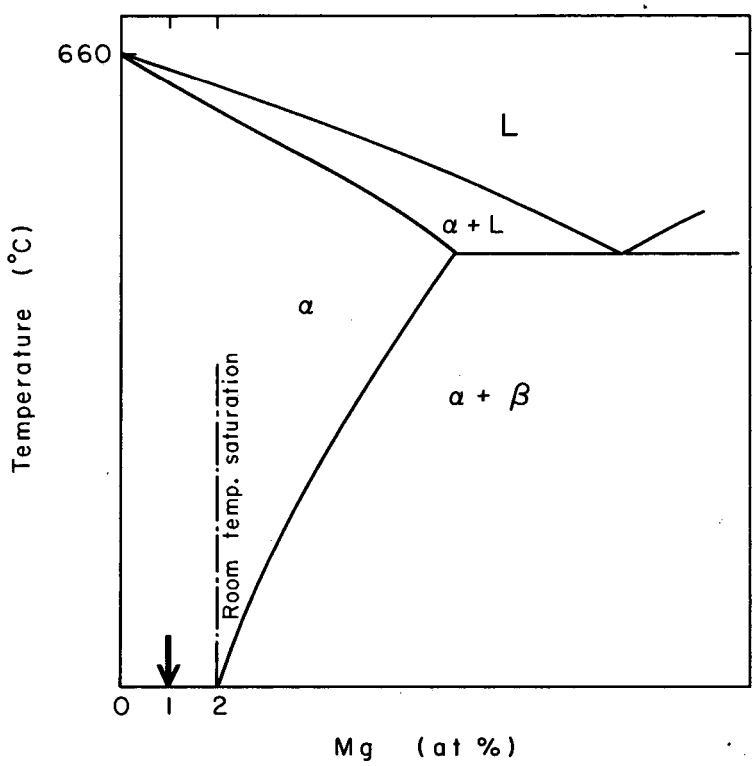
660
L
α + L
α
α + β
Room temp. saturation
Temperature (°C)
0
1
2
Mg (at %)
MU-35237

Fig. 1

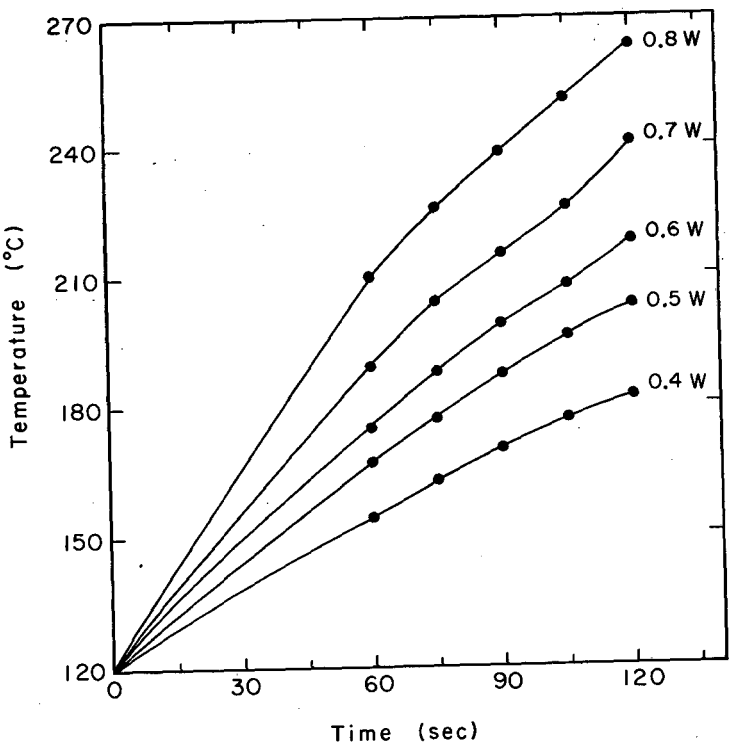
270
240
210
180
150
120
Temperature (°C)
0
30
60
90
120
Time (sec)
0.8 W
0.7 W
0.6 W
0.5 W
0.4 W
MU-35238

Fig. 2

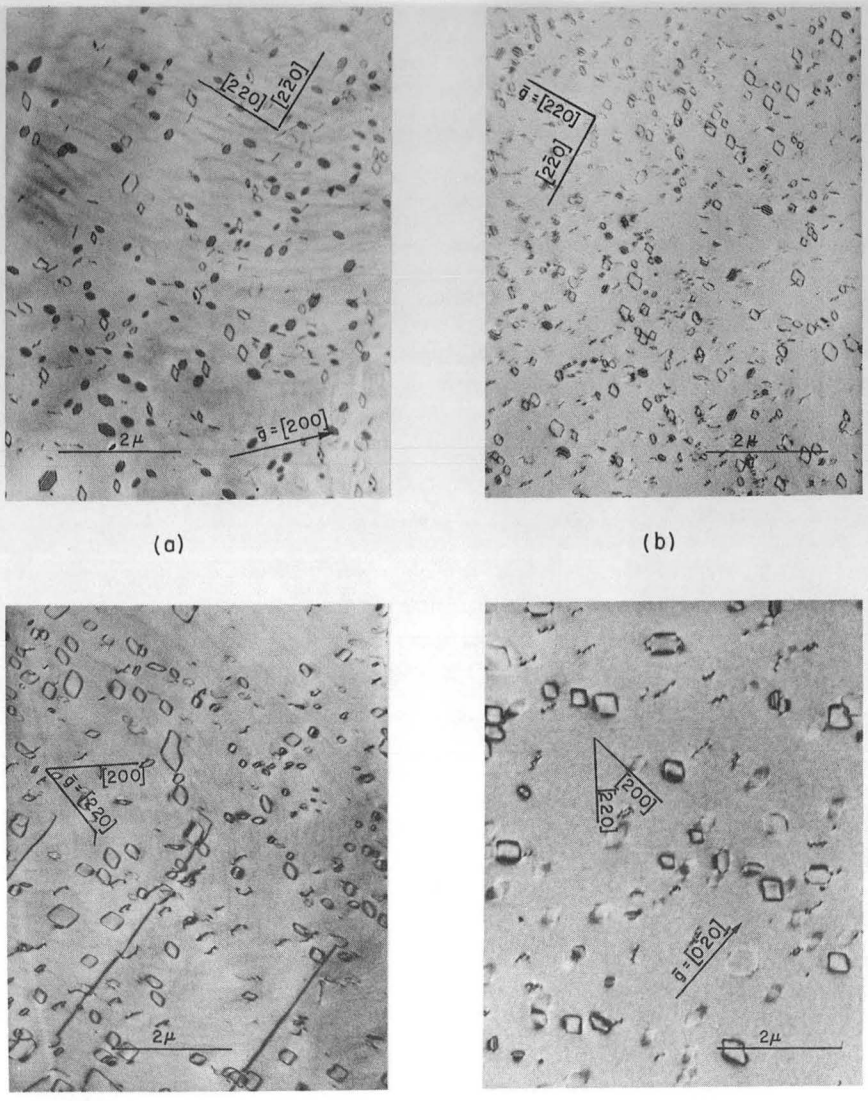
[220]
[2$\bar{2}$0]
$\vec{g}$=[200]
2μ
(a)
$\vec{g}$=[220]
[22$\bar{0}$]
2μ
(b)
[200]
$\vec{g}$=[3$\bar{2}$0]
2μ
(c)
[200]
[220]
$\vec{g}$=[0$\bar{2}$0]
2μ
(d)

ZN-4823

Fig. 3

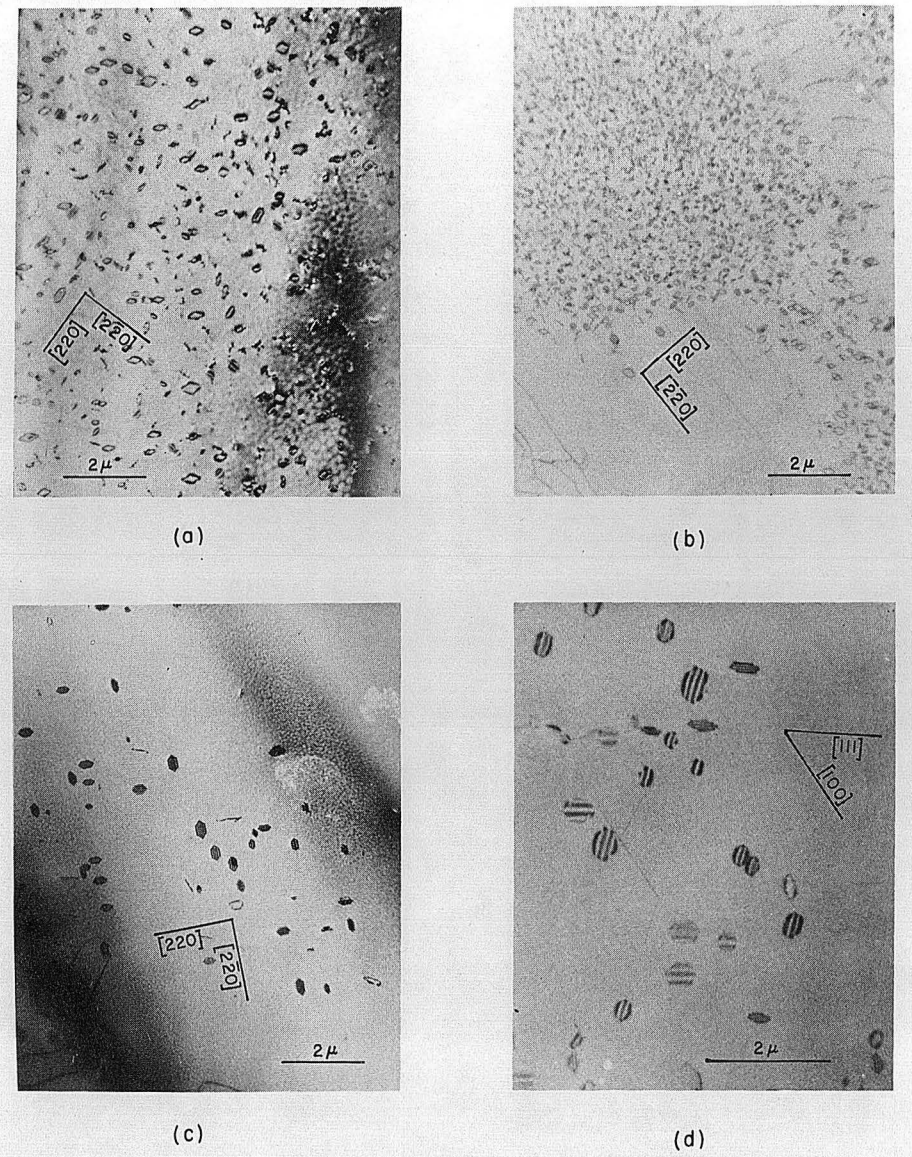

ZN-4822

Fig. 4

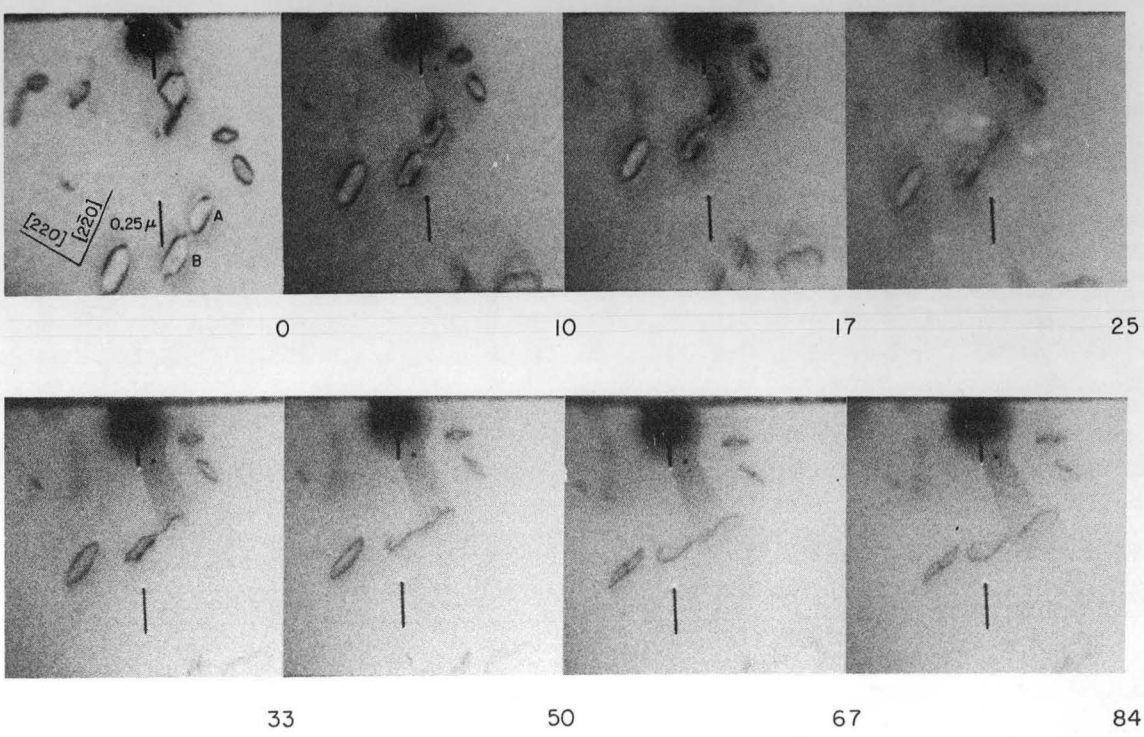

Fig. 5

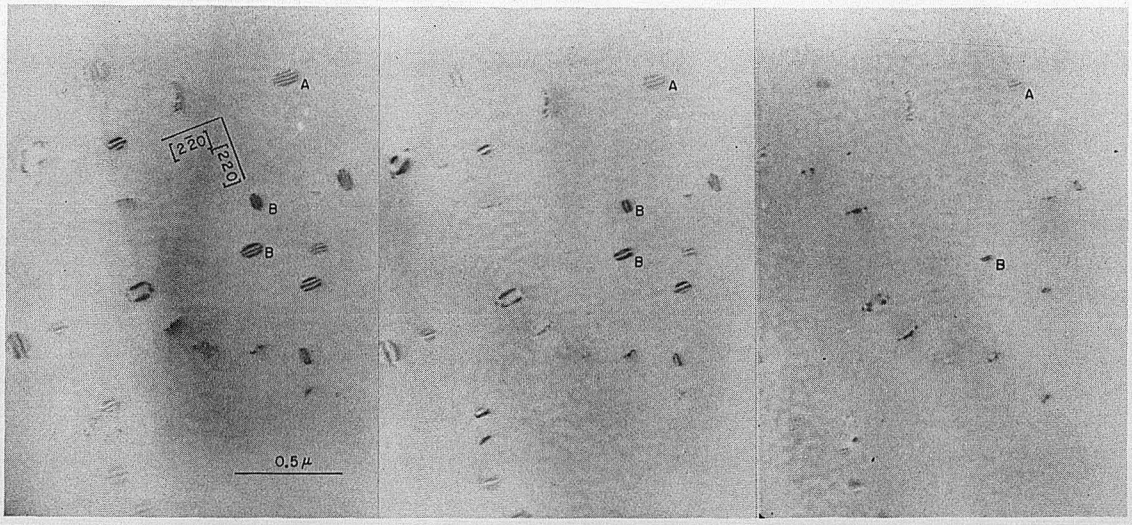

(a) 0 (b) 60 (c) 75

ZN-4818

Fig. 6

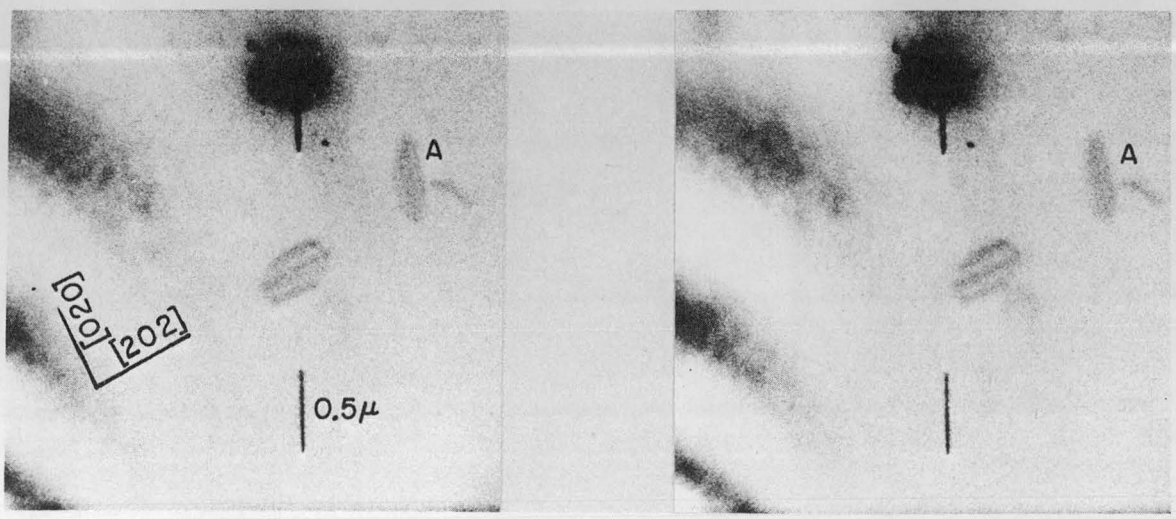

(a) 0 (b) 3

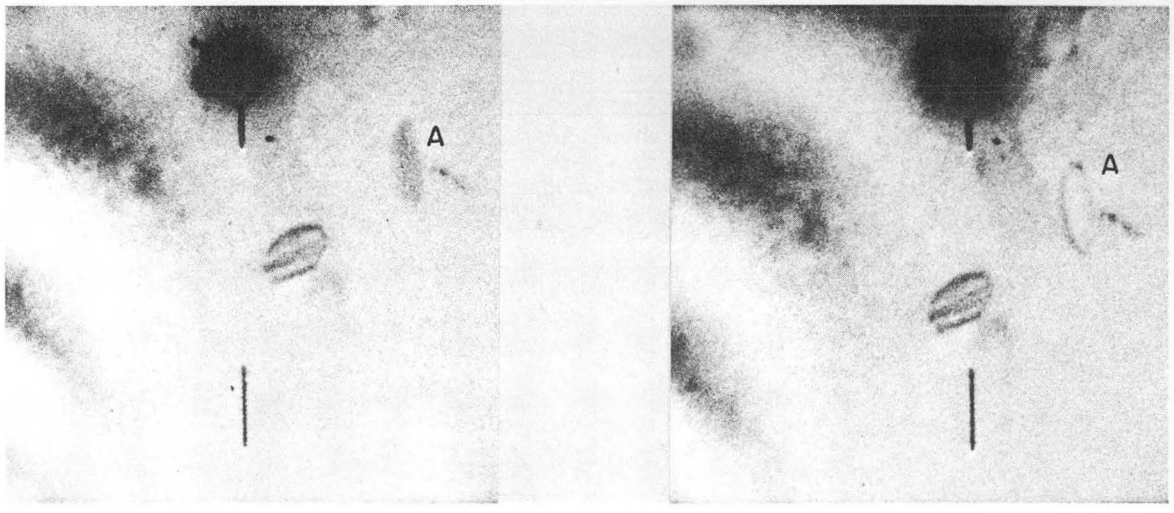

(c) 7 (d) 10

ZN-4821

Fig. 7

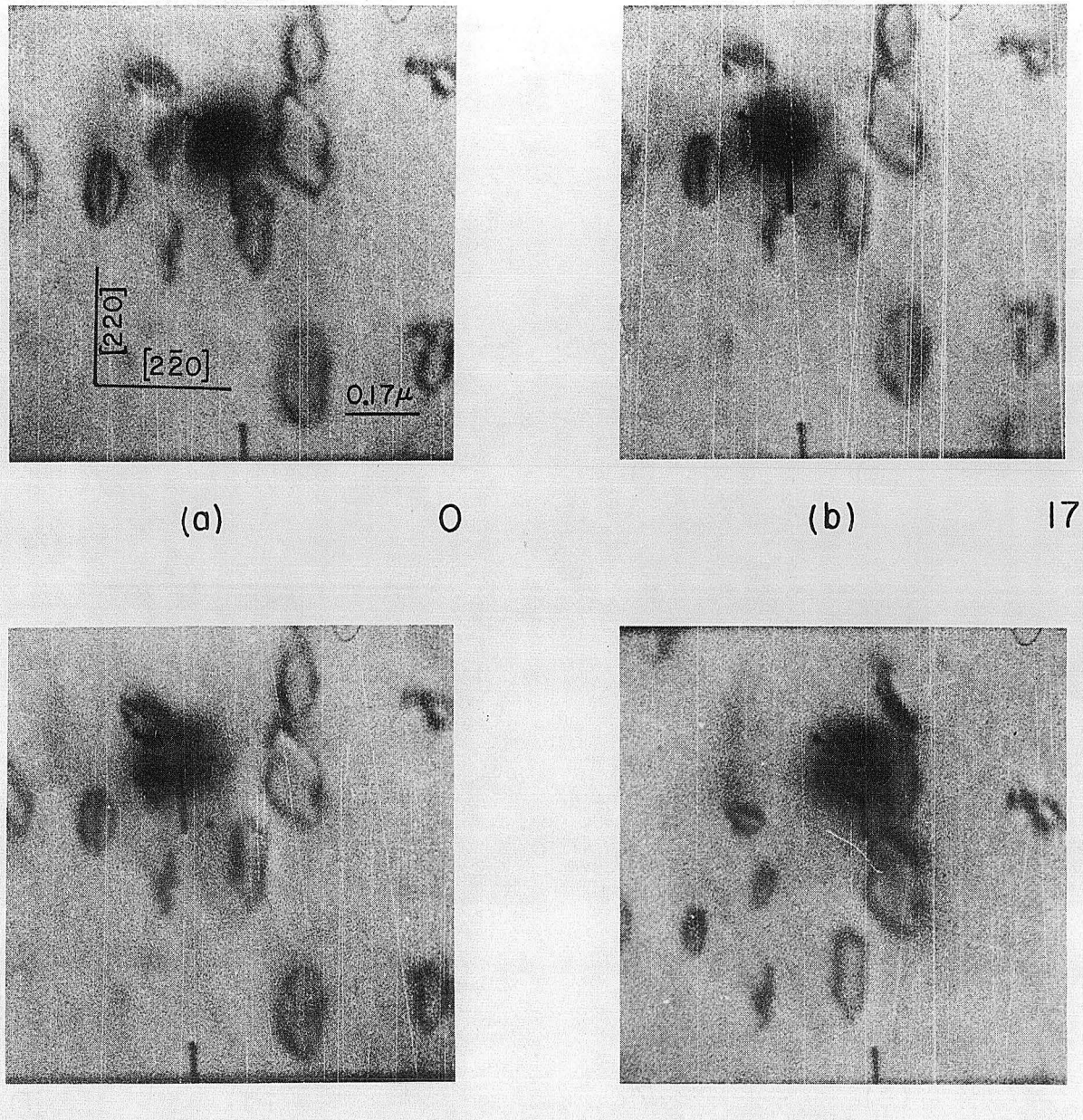

Fig. 8

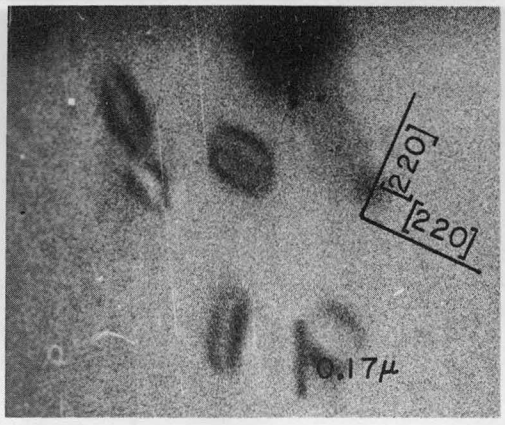

(a) 0

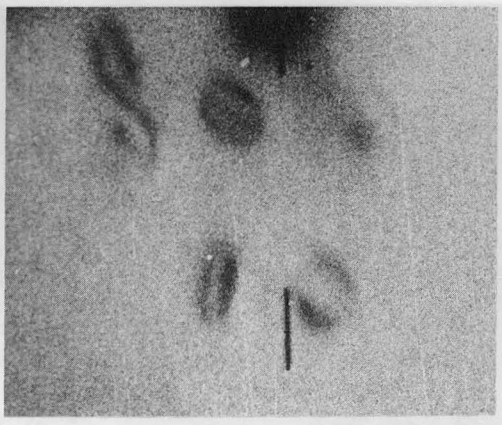

(b) 23

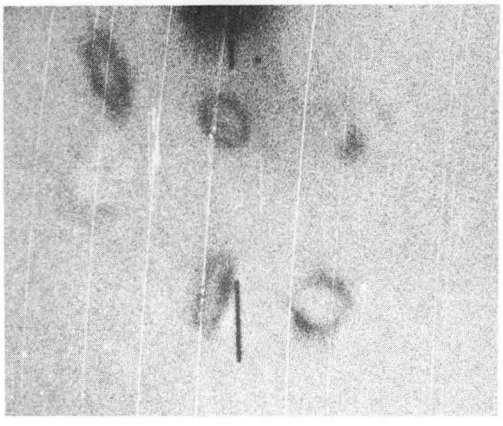

(c) 43

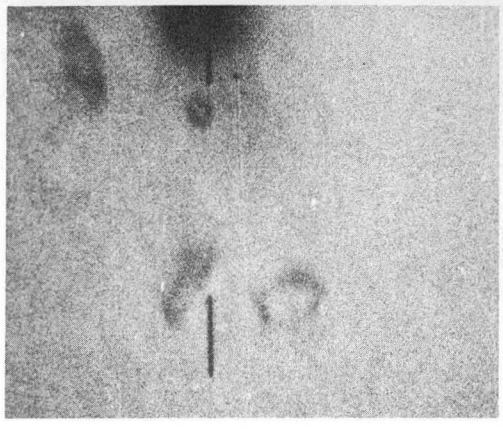

(d) 50

ZN-4820

Fig. 9

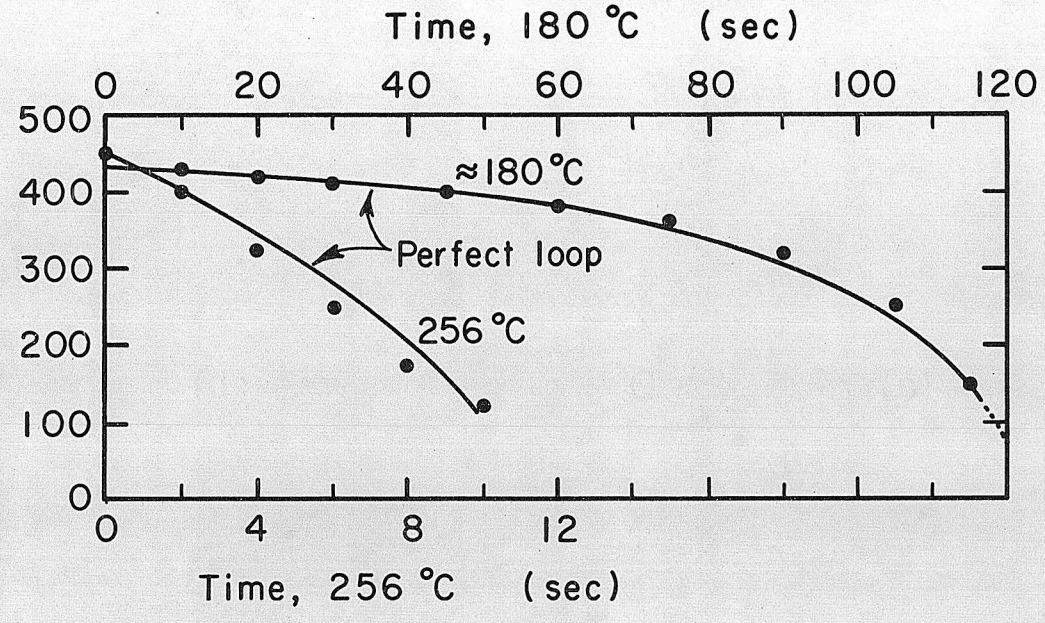

MU-35235

Fig. 10a

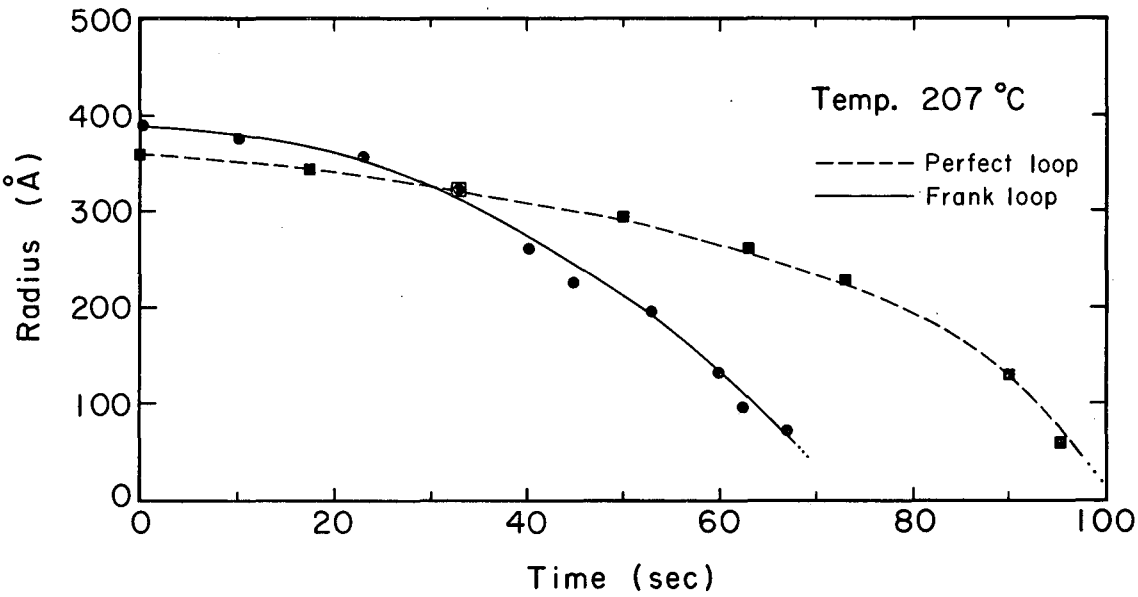
500
400
300
200
100
0
Radius (Å)
0
20
40
60
80
100
Time (sec)
Temp. 207 °C
Perfect loop
Frank loop
MU-35239

Fig. 10b

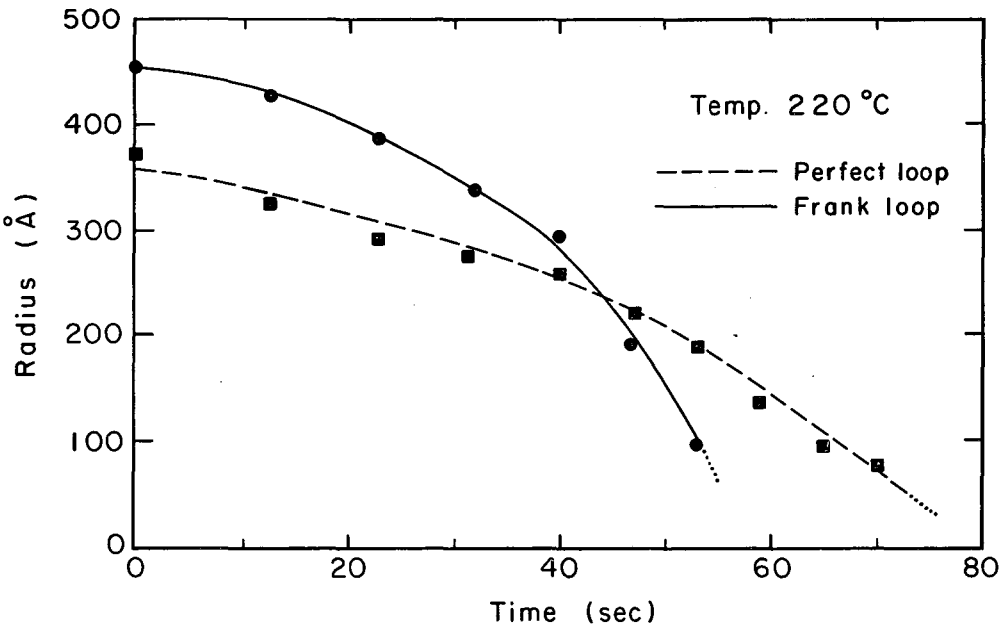
500
400
300
200
100
0
Radius (Å)
0
20
40
60
80
Time (sec)
Temp. 220 °C
Perfect loop
Frank loop
MU-35236

Fig. 10c

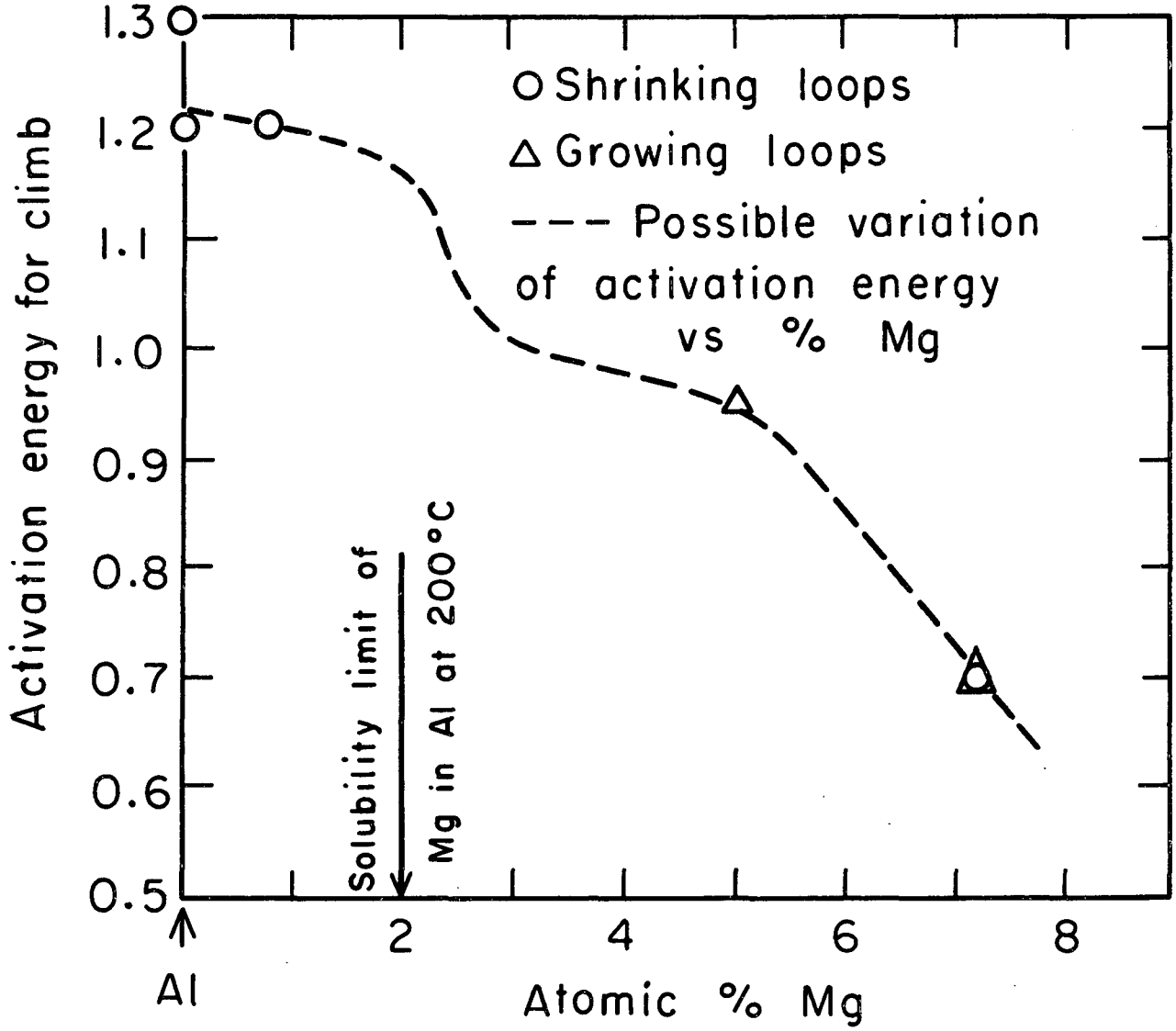

MUB-5171

Fig. 11